Materials and Design 168 (2019) 107650

Contents lists available at ScienceDirect

Materials and Design

journal homepage: www.elsevier.com/locate/matdes

Learning from nature: Use material architecture to break the performance tradeoffs

Zian Jia [a], Yang Yu [a,b], Lifeng Wang [a,*]

[a] Department of Mechanical Engineering, State University of New York at Stony Brook, Stony Brook, NY 11794, USA
[b] Department of Mechanics, School of Aerospace Engineering, Beijing Institute of Technology, Beijing 100081, China

HIGHLIGHTS

- "Strong and tough", "strong and compliant", "stiff and dissipative", and "flexible and responsive" architected materials are designed, breaking the performance tradeoffs in bulk materials.
- The dynamic performances of five bioinspired microstructures are compared.
- Quantitative material indices are proposed to characterize the material's overall performance.
- Combining hierarchical designs with hybrid designs results in better impact resistance.

GRAPHICAL ABSTRACT

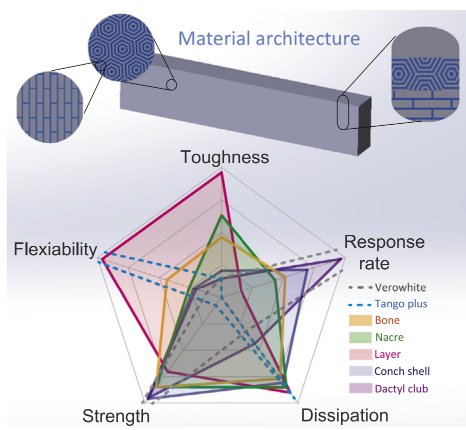

ARTICLE INFO

Article history:
Received 13 October 2018
Received in revised form 8 February 2019
Accepted 9 February 2019
Available online 12 February 2019

Keywords:
Structure-property relationships
Performance tradeoffs
Biomimetics
Architected materials
Hierarchical materials

ABSTRACT

In material science, the enhancement of a specific material performance is often accompanied by undermining another material property, notoriously known as the performance tradeoffs, such as that between strength and toughness, stiffness and energy dissipation, and flexibility and fast response. Free combinations of material properties that go beyond these performance tradeoffs are highly desirable in areas as diverse as civil engineering, soft robotics, armor designs, and reconfigurable metamaterials. Learning from nature, we 3D print architected materials with bio-inspired microstructures that successfully surpass the above performance tradeoffs. The integration of microstructural elements on multiple length scales (hierarchical designs) and on one specific length scale (hybrid designs) are further discussed and compared. Through experimental and theoretical analysis, we reveal that the performance enhancements stem from the material architecture's significant manipulation over the deformation field, crack location, and crack pattern. This study on the relationship between material microstructure and material performance will aid architected material design with ideal combinations of mechanical properties.

1. Introduction

From artificial tissues [1], soft robotics [2], and wearable electronics [3] to armors [4], spacecrafts [5], and constructions [6], many systems require materials with certain property combinations of stiffness/

* Corresponding author.
E-mail address: lifeng.wang@stonybrook.edu (L. Wang).

https://doi.org/10.1016/j.matdes.2019.107650

flexibility, strength, toughness, energy dissipation, and fast response. While some material properties, like stiffness and strength, can be readily improved together, many other properties (such as strength and toughness [7], flexibility and strength [8], stiffness and energy dissipation [9–11], and flexibility and fast response [12]) are mutually exclusive. This is known as the material performance tradeoffs, which limits the creation of novel materials with desirable performance profiles and stays as a major obstacle for filling the "holes" in the material property space [13].

In the efforts of pushing the material properties beyond the performance tradeoffs, two main strategies have been adopted. The traditional approach creates monolithic bulk materials by modifying the atomic or molecular compositions at the sub-nanometer scale largely depends on trials and errors and thus inefficient [13]. Recently, the architected material approach – control of the material microstructure – has attracted increasing attention [14–17], facilitated by novel material fabrication technologies like self-assembly [18–21] and 3D printing [22–27]. Learning from nature, architected materials have been successfully adopted to break the tradeoff between strength and toughness [7,28]. For example, strong and ductile metals are generated by alternatively distributing coarse grain layers and ultrafine grain layers at the micrometer scale [29], similar to the layered structure in sea sponges [30]. Tough ceramics are designed by staggering ceramic plates in a "brick and mortar" architecture [31–33] mimicking nacre [34,35]. While the tradeoffs between strength and toughness are well understood, other tradeoffs between compliance and strength, stiffness and dissipation, and flexibility and response rate remain largely unexplored [9–11]. On the other hand, recent progress in flexible armors, deployable devices, and soft robotics, have posed new requirements on properties like dissipation, flexibility, and response rate under dynamic loading conditions [36,37]. Thereby, aside from breaking the performance tradeoffs between two properties, we also aim to produce architected materials with balanced (or simultaneous enhanced) multiple dynamic properties, as depicted in Fig. 1.

Biomaterials provide great inspirations for designing architected materials [33,38,39]. Their design strategy has been revealed as building intricate architectures from relatively simple structural elements [40–42]. Using 3D printing, various bioinspired microstructural elements have been reproduced and studied, including nacre inspired staggered structure [43–46], sea shell inspired cross-lamellar structure [47], bone osteon inspired cylindrical network structure [48,49], and stomatopod inspired rotating plywood structure [50,51]. A systematic comparison between different microstructures is not yet available. Moreover, most previous studies report the properties under static loading conditions [1,22,44,52].

Furthermore, different structural elements are assembled into hierarchical structures and/or gradient structures to obtain better material performances. The first strategy is hierarchy, which replaces microstructure with higher order sub-microstructures spanning multiple length scales [52]. Examples include bones [53–55], sea sponges [30], and collagen fibers [56]. The material gradient strategy, by contrast, integrates different microstructures at one specific length scale. This strategy is ubiquitous in biological protection systems like brains [57], abalone shells [34], fish scales [34,58], and stomatopod clubs [59]. Compared to the broad interest in 3D printing hierarchical materials [52,60–65], 3D printing hybrid materials have attracted less attention [66–68].

In this study, the dynamic performance of layered, brick and mortar, concentric hexagon, cross-lamellar, and rotating plywood microstructures are first compared. How these microstructures overcome the performance tradeoffs are discussed. Furthermore, more intricate architectures are produced by integrating these microstructural elements. The hierarchical design, hybrid design, and the combination of hierarchy and hybrid design are investigated. The resultant material property space is visualized in Ashby plots, highlighting the role of material architecture in breaking the performance tradeoffs.

2. Methods

2.1. Microstructure design

The basis structural elements studied here are the layered, brick and mortar, concentric hexagon, cross-lamellar, and rotating plywood microstructures, mimicking that of sea sponge, nacre, bone osteon, conch shell, and stomatopod dactyl club, respectively. The geometries are presented in Fig. 2, and the modeling details are provided in Supplementary Material. Although not all-inclusive, these microstructures represent

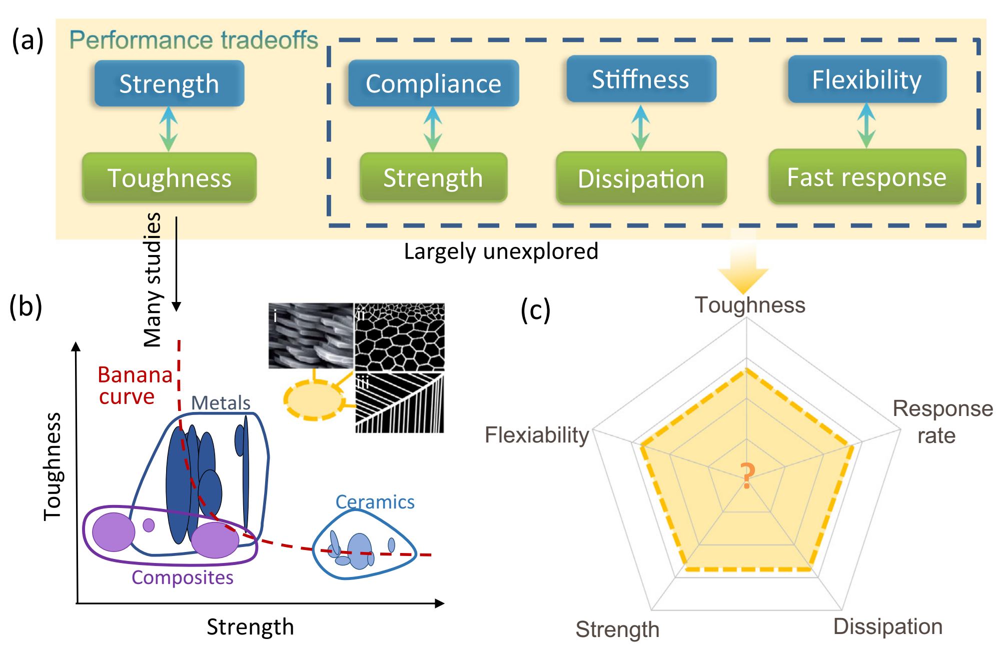

Fig. 1. The material performance tradeoffs. (a) Material properties that are typically exclusive. (b) The performance tradeoff between strength and toughness is tackled by materials with (i) staggered plate microstructure [31,32], (ii) alternating coarse grain and fine grain microstructure [29], and (iii) nano-twined lamellar microstructure [69]. (c) Research areas like soft robotics, wearable devices, and reconfigurable metamaterials present new requirements on material properties, e.g., an ideal combination of flexibility, strength, toughness, energy dissipation, and fast response.

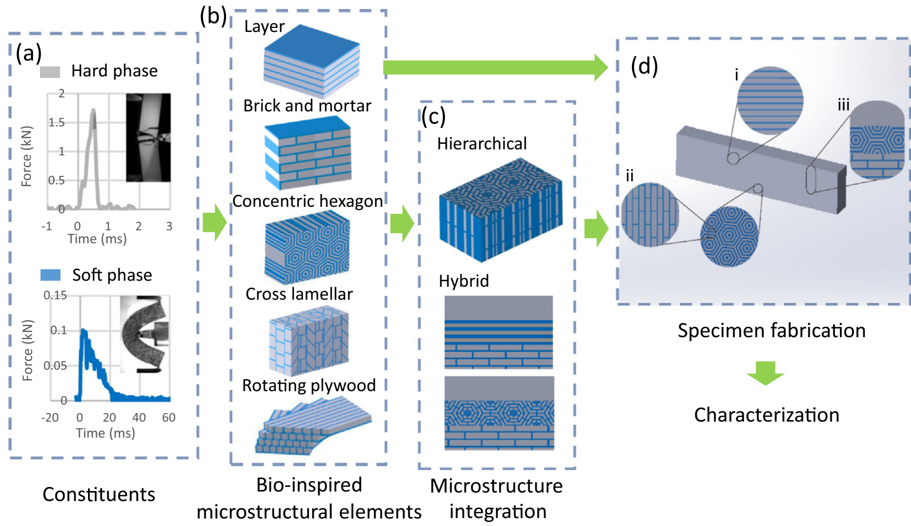

Fig. 2. The design motif of architected beams. (a) The force histories of the constituent materials under impact. The incident velocity is 3.4 m/s. (b) The layer, brick and mortar, concentric hexagon, cross-lamellar, and rotating plywood microstructural elements. (c) Integration of the microstructural elements with a hierarchical approach (top) and a hybrid approach (bottom). (d) The architected beam specimens are then printed with (i) a specific structural element, (ii) hierarchical microstructure, and (iii) hybrid microstructure.

the constituent structural elements in biomaterials. For example, the hierarchical architecture of bone is an assembly of these microstructures at different length scales (Fig. S2, Supplementary Material). Using these basis elements, the architected beams are then constructed 1) using one specific bioinspired microstructural element, 2) integrating several microstructural elements over multiple length scales (the hierarchical design), and 3) integrating microstructural elements at a specific length scale (the hybrid design). The soft phase volume fraction of all microstructures is controlled to be 0.25 (consistent with [47], representing a relative high mineralization level), except that of the bone osteon inspired structure is 0.50 (representing a moderate level of mineralization [48,70,71]). Note that the geometric parameters of the brick and mortar microstructure are designed such that microcracking take place under impact. Specifically, the concentric multilayer structure is an important feature of bones osteons, which can also be found in biomaterials like tree annual rings, sea sponges, and bamboos. Focusing on the concentrically layered feature, we propose concentric hexagonal units to occupy the whole plane. For readers interested in the circular shape design of bone osteon, reference [49] can be referred to. The geometric parameters of the concentric hexagonal microstructure are calculated such that crack deflection around the hexagons takes place [72]. All geometric sizes are provided in Table S1, Supplementary Material.

2.2. Dynamic three-point bending tests

The specimens used in the dynamic tests are $18 \times 88 \times 8$ mm^3 beams printed using a commercial Objet Connex260 3D printer (Stratasys Corporation). The printer prints multi-material simultaneously and has a print precision of 30 μm in the layer direction and 43 μm (600DPI) in the other two directions. The two base materials are a soft rubbery material (Tango Plus) and a hard-glassy polymer (VeroWhite, flexural strain of failure ≈0.03 at an impact velocity of 4 m/s). The dynamic tests are performed using a modified split Hopkinson pressure bar (SHPB) system with impact velocity in the range of 2–12 m/s. In this velocity range, the glassy polymer breaks catastrophically with ignorable plastic deformations while the rubbery polymer stays flexible, similar to the mechanical performances of bio-minerals and biopolymers. The bending span is 72 mm (span to depth ratio = 4, ensuring small end effect in the middle) and the impactor mass is 335.26 g. The impact duration is recorded by a high-speed videoing system (Photron SA1.1) with 15,000 frames per second, from which the displacement and velocity history of the impactor are obtained. The strain fields are calculated by digital image correlation (DIC) using the commercial software VIC-2D (Correlated Solution Inc.).

2.3. Dynamic performance characterization

The flexural stiffness, energy dissipation, and response time are calculated at a relatively small incident velocity (3 m/s) before damage takes place. The energy dissipation ratio is estimated as the fraction of kinetic energy loss after impact, $1-(V_{res}/V_{ini})^2$, where V_{ini} and V_{res} are the initial and residual velocity of the impactor. Note the energy dissipation ratio is proportional to the loss tangent typically used for viscoelastic characterization (Supplementary Material Section 4). The response time (τ) is evaluated as the time required for the beam to push the impactor back at certain incident energy. The shorter the response time, the faster the response. Therefore, the response rate is proportional to $1/\tau$.

The critical values related to failure, i.e., critical velocity, critical strength, and critical energy, are obtained by gradually increasing the impact velocities until the breakage of the specimen (Fig. 3a). The critical energy absorption ($E_{ab} = mV_{ini}^2/2 - mV_{res}^2/2$, m is the mass of the impactor) and the critical failure force are used as indicators for the toughness and strength. A schematic of how these parameters are obtained is shown in Fig. S3, Supplementary Material.

3. Results and discussion

3.1. Comparison between different structural elements

The dynamic performance of the microstructural elements is characterized first. Fig. 3b–e plot, respectively, the dissipation ratio, response time, critical velocity, and critical failure energy of different structural elements. Compared to the constituents, moderate performance improvements and distinct performance profiles are observed. For instance, the layered microstructure shows the highest dissipation and the highest critical energy, but relatively long response time and low stiffness. The strain field obtained by digital image correlation (DIC) reveals that its high flexibility and energy absorption originates from extensive shear deformations (Fig. S8). Theoretical analysis (Supplementary Material, Section S4) confirms the competition between tensile deformation and shear deformation in architected materials, which shows that shear dominant deformations typically lead to

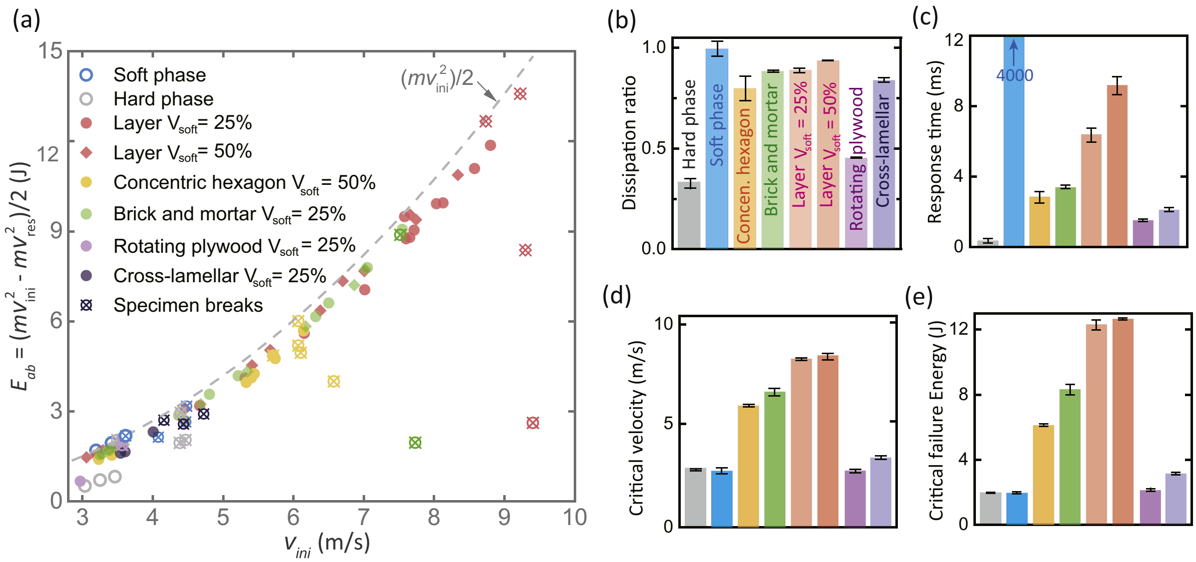

Fig. 3. A comparison of the dynamic performance between different bioinspired microstructures. (a) The energy absorption plotted against impact velocity. The symbols with x indicate the break of the specimen. (b–e) show the dissipation ratio, response time, critical velocity, and critical failure energy, respectively.

higher dissipation. The analysis also reveals that response time is proportional to $1/\sqrt{(1-\eta)}$. Thereby, a dissipation ratio (η) close to 1 leads to a long response time, which explains the slow response of the layered specimen. Moreover, the layered specimens with $V_{soft} = 0.25$ and $V_{soft} = 0.5$ show similar performances, suggesting that the microstructure plays a dominant role.

Compared to the layered microstructure, the rotating plywood and cross-lamellar microstructure are stiffer and more responsive. The critical failure energy of the cross-lamellar structure improves 50% compared to the hard phase, consistent with previous drop tower results (85%) [47]. Unexpectedly, the 3D printed rotating plywood specimens show no improvement in critical failure energy (Fig. 3e), different from the results reported in stomatopod dactyl clubs [59]. The explanation is as follows. In the stomatopod, the rotating plywood structure is located in the middle layer of the club working synergistically with its curvy shape. Thus, the rotating plywood region is largely in compression and serves the function of arresting cracks rather than preventing crack initiation. Based on such observation, we assume that the rotating plywood structure is a good crack propagation arrester, but a poor crack initiation stopper. To verify this, we performed an additional compact tension (CT) fracture test of the rotating plywood microstructure (Fig. 4). The crack resistance curve (R curve) is calculated referring to the ASTM standard E1820. Interestingly, a "J" shaped R curve is obtained, presenting a relatively low fracture resistance at crack initiation (2.5 KJ/m^2). But the energy required to extend the crack increases rapidly, which reaches 15 KJ/m^2 at a crack length of 12 mm. Such a "J" shaped R curve makes the rotating plywood structure a perfect crack arrester. However, the low crack initiation toughness makes it prone to crack initiation and premature cracking, which is observed in our dynamic three-point bending tests (Fig. S8). Nevertheless, the crack arresting ability together with merits like high stiffness and low dissipation makes it preferable in biomaterials such as teeth, teleost scales, beetle cuticle, and the center layer of stomatopod dactyl club [59,73–75]. In biomaterials, the arrested microcracks help to avoid catastrophic damage, which can be self-healed at favorable environment conditions [76].

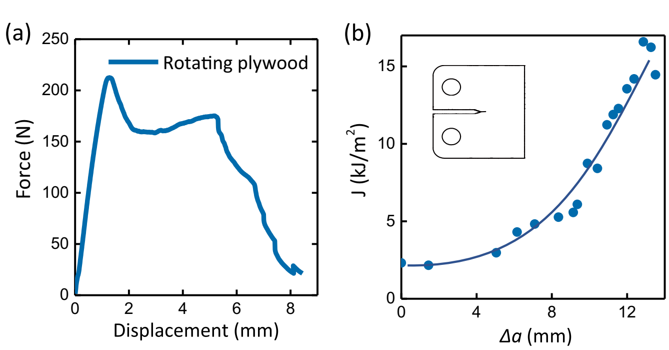

Fig. 4. CT fracture test of the rotating plywood microstructure. (a) Experimentally measured force vs displacement curve. (b) The "J" shaped crack resistance curve.

The concentric hexagonal structure and the brick and mortar structure show a better-balanced performance, having no significant shortcomings. As a result, they are relatively robust microstructures, which rationalize their ubiquity in nature. More specifically, the bone osteon inspired (or nacre inspired) structure is 140% (165%) more dissipative, 270% (116%) more flexible, and 200% (319%) tougher than the hard phase. Compared to the soft phase, the bone osteon inspired (or nacre inspired) structure is 15 (20) time stiffer, 10 (10) times stronger, 2.5 (3.3) times tougher, and response 1000 (1000) times faster, with less than 20% (11%) reduction in the energy dissipation. Further strain field observations reveal that both structures possess highly localized strains and distributed microcracking (Fig. S9, more information in [77]). The results indicate that the ability to accommodate deformations into the soft phase at high strain levels without catastrophic damage is important for balanced performances. The underlying physics of the balanced dynamic performance can be understood as following: 1) the localized strain magnifies deformation in the soft phase, which contributes to higher dissipation, 2) the localized strain lead to higher stress levels, which contributes to higher strength and faster response, and 3) the delocalized microcracks prevent catastrophic damage and facilitate a larger fracture process zone, which contributes to better toughness. Such mechanisms are extensions to the statement that an energy dissipation mechanism with locally high stress is crucial for overcoming the conflict between strength and toughness [7].

3.2. Radar plot visualization and overall performance evaluation

To give a better visualization of various material properties, Fig. 5a plots the performance profiles in a radar plot similar to previous studies [48,78,79]. Each material property is normalized by the

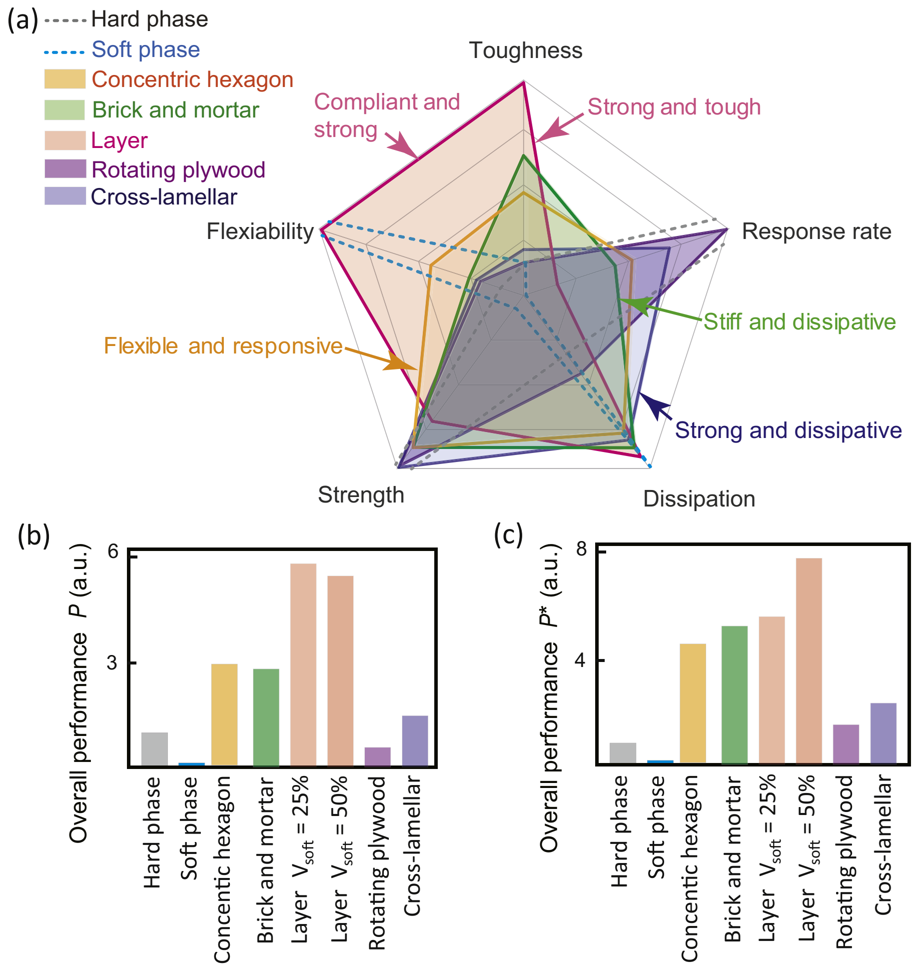

Fig. 5. (a) Visualization of flexibility, strength, toughness, energy dissipation, and response rate in a radar plot. (b) and (c) show overall performance characterized by P (suitable for soft actuators and wearable electronics) and P^* (suitable for structural components and armor designs), respectively. All the values are normalized.

maximum value of the bioinspired structure element. For instance, the cross-lamellar structure shows the maximum strength (among all bioinspired structures), its strength is used for normalization. In addition, because the dissipation ratio is itself dimensionless, it is plotted directly. The results show that compliant and strong, stiff and dissipative, strong and dissipative, and flexible and responsive performances are achieved by the layer, brick and mortar, cross-lamellar, and concentric hexagonal microstructure, respectively. Importantly, the bone osteon inspired concentric hexagon structure shows a good performance balance.

In order to further give a quantitative characterization of the material's overall performance including multiple properties, material indices similar to that proposed by Ashby [80] is adopted. For instance, the overall performance can be straightforwardly represented by the enclosed polygon area in the radar plot. Analogy to this, a comprehensive parameter is proposed by multiplying the normalized flexibility ($1/K$), dissipation ratio (η), strength (σ_f), toughness (E_{ab}), and response rate ($1/\tau$) as follows

$$P = \frac{\eta}{\eta_0}\frac{\tau_0}{\tau}\frac{\sigma_f}{\sigma_{f0}}\frac{K_0}{K}\frac{E_{ab}}{E_{ab0}}, \quad (1)$$

where K is the flexural stiffness and τ is the response time. The subscript 0 denotes the material property of the hard phase. The proposed parameter P is suitable for applications like soft actuators and wearable electronics, where flexibility and fast response are of great importance. By contrast, in structural components and skeleton designs, stiffer, stronger, tougher, and more ductile materials are preferred. In such scenarios, another performance parameter can be proposed as

$$P^* = \frac{K}{K_0}\frac{\sigma_f}{\sigma_{f0}}\frac{E_{ab}}{E_{ab0}}\frac{\eta}{\eta_0}\frac{\Delta_{\max}}{\Delta_{\max 0}} \quad (2)$$

where Δ_{max} is the maximum displacement at failure. The values of P and P^* for different structures are presented in Fig. 5b and c, respectively. Results show that the layer microstructure element exhibits the best overall performance. The maximum improvement of P and P^* reached 405% and 664%, respectively.

In addition, for given applications, more specific material indices should be used. For example, in a vibrational beam design for minimum flexural excitation, the material index can be derived as $\eta K^{1/2}/\rho$ [80], with ρ denoting the effective density. In which case, the microstructure that maximizes $\eta K^{1/2}/\rho$, the cross-lamellar microstructure, should be selected.

3.3. Hierarchical design

So far, we've characterized five bioinspired structural elements and proposed an approach to select between these elements. The performance, however, can be further improved by integrating the basic elements into more intricate material architectures. To demonstrate the role of hierarchy, we design a hierarchical microstructure, mimicking the staggered structure of collagen fibrils [70]. The modeling of the microstructure is shown in Fig. 6. The volume fraction of the hierarchical concentric hexagonal design is controlled to be the same as the regular

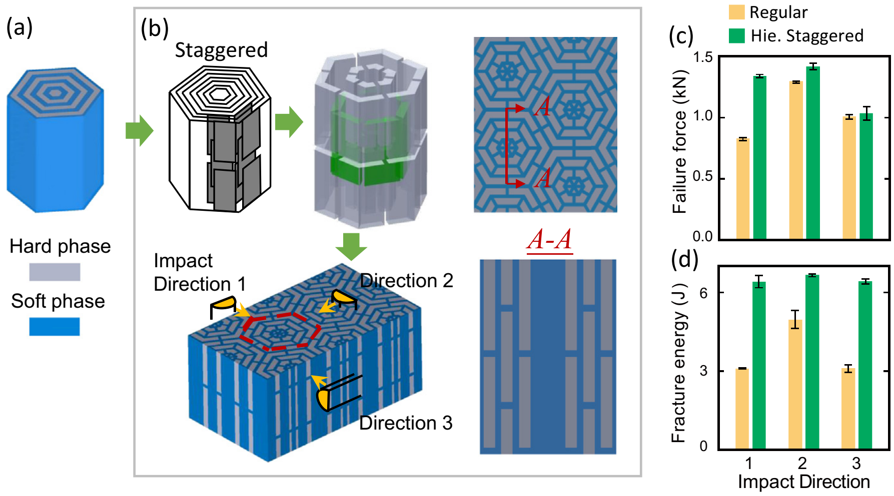

Fig. 6. Hierarchical design. (a) The regular concentric hexagon unit cell. (b) The staggered hierarchical design mimics the staggered microstructure of the collagen fibrils. On the right shows the top view and cross section view. The impact directions with respect to the unit cell are highlighted. (c) and (d) show the effect of hierarchy on material strength and toughness.

concentric hexagonal microstructure ($V_{soft} = 0.5$). The dynamic performance is then evaluated from three orthogonal directions as depicted in Fig. 6b. Compared to the regular concentric hexagonal structure, the proposed hierarchical design shows simultaneously improved failure force and fracture energy in all impact directions (Fig. 6c). The maximum improvement reaches 60% in failure force and 100% in fracture energy. Previous theories have proven that simultaneously improved strength and toughness are not available in self-similar hierarchies [56,70,81]. As a supplementary, our results show that proper (necessarily different) microstructures at different hierarchical levels are essential to achieving simultaneously improved strength and toughness. Our DIC results further reveal that the enhanced dissipation, strength, and toughness originates from more extensively distributed microdamage and an inclined "flexural shear crack" penetrating more soft phase materials (Fig. S9, Supplementary Material).

3.4. Hybrid design

Although hierarchy improves strength and toughness simultaneously, high levels of hierarchy poses significant challenges for fabrication. On the one hand, we should continue pursuing novel fabrication techniques that can span multiple length scales. On the other hand, we should consider alternative approaches that can provide a wider design space without laying too strict constraints on fabrication. The hybrid design – assembly of microstructures at a specific length scale, may provide one alternative solution to hierarchy. Fig. 7a shows a schematic of hybrid designs, usually accompanied by material gradients.

To this end, we design and investigate gradient hybrid microstructures. The specimens are simplified to have three layers. Fig. 7a presents four hybrid designs. Design 1 and Design 2 mimics the strategy of stomatopod and abalone shell, where the first hard layer provides stiffness and prevents penetration, the second layer is crack tolerant and serve as a crack arrester, and the third layer uses a microcracking mechanism to dissipate as much impact energy as possible. Design 3 and Design 4 are based on the layered microstructure, with a concentric hexagon and a hard phase layer for reinforcement, respectively. Specifically, Design 3 uses the concentric hexagonal layer to provide a microcracking mechanism, and Design 4 uses a mono-hard layer to resist shear deformation. A summary of the hybrid designs is provided in Table S3. Note that

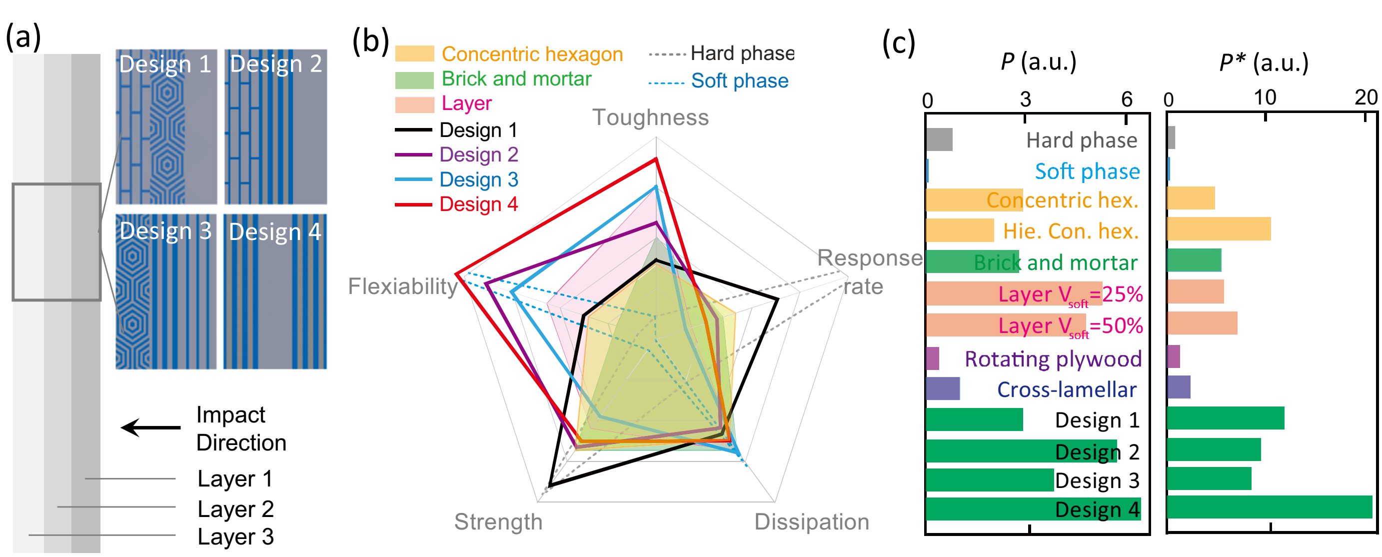

Fig. 7. (f) Four hybrid designs where the specimens are simplified as three layers, introducing extra control over the strain distribution and fracture pattern. (g) Radar plot demonstrating the performance of the hybrid designs compared to the basis structural elements. (h) The overall performance comparison between different micro-architecture designs. P and P^* are defined in Section 3.2.

because of the size limit incurred by our 3D printer, each layer does not have enough unit cells in a homogeneous point of view. Nevertheless, they serve the goal of demonstrating the potential of hybrid microstructural design.

Fig. 7b and c present the dynamic performance of the hybrid designs in comparison with the bioinspired structural elements. The hybrid designs demonstrate impressive performance enhancements. For example, Design 1 improves stiffness (85%), strength (32%), and response rate (53%) significantly compared to the bone osteon microstructure, while the dissipation and flexibility stay about the same. All the properties of design 4 are enhanced compared to the layered microstructure. To quantitatively compare between different architecture design strategies, Fig. 7c plots the overall performance evaluated by P and P^*. Results demonstrate the hybrid designs as a promising replacement for hierarchical designs. The overall performance P of hybrid Design 4 is about 3 times of the hierarchical design, and P^* is about 2 times of the hierarchical design.

Aside from the performance improvements, more controls on the strain field and fracture pattern are achieved with hybrid designs. For instance, the deformations can be localized into a single layer or a combination of several layers. As a result, the location of crack initiation and the pattern of crack propagation can be controlled (Fig. 8). Rich and interesting cracking patterns, such as crack initialized by microcracking (Fig. 8b), crack propagate with crack branching (Fig. 8e), and crack slowed down by crack blunting (Fig. 8d) are observed. For instance, Design 4 shows an interestingly crack path – the crack initiates from the center at layer 2, which then penetrates layer 3, and finally propagates towards layer 1 with crack branching (Fig. 8e). Such a complex cracking pattern brings a dynamic critical failure energy improvement of 640%, 8 times larger than the best improvement previously reported in 3D printed architected materials (85%) [47]. It should be noted that the previous study uses a different test set up (drop tower), the comparison here is demonstrated as a qualitative reference. Moreover, compared to the catastrophic fragmentation of the hard material (Fig. 8a), the hybrid designs fail progressively (Fig. 8b–d). The progressive damages are more controllable which are facilitated for two reasons: first, the improved crack arresting ability of bioinspired microstructures; second, the kinetic energy is released at the layer interfaces with mismatched effective modulus [77]. The strain field distributions are shown in Fig. S10 and more discussions of the toughening mechanisms can be found in Ref [77].

3.5. Combining hierarchical design with hybrid design

The above results show that hybrid design is a simple yet effective approach to enhance the material's dynamic performance. Note that the improvements in the hierarchical design are not as significant as the hybrid design because the specimens are created with only two levels of hierarchy. Yet, more significant improvements can be envisioned with higher hierarchy levels. On the other hand, in situations when the maximum hierarchy level is limited by the fabrication techniques, one applicable solution is to combine low order hierarchical design with the hybrid design. An example is demonstrated in Fig. 9, where the middle layer of hybrid design 1 is replaced with its hierarchical counterpart proposed in Section 3.3. We found that while the original hybrid specimen cannot stop the crack at an impact velocity of 6.30 m/s, the hierarchical hybrid design successfully captures the crack at an impact velocity of 6.51 m/s (breaks at 6.88 m/s). The

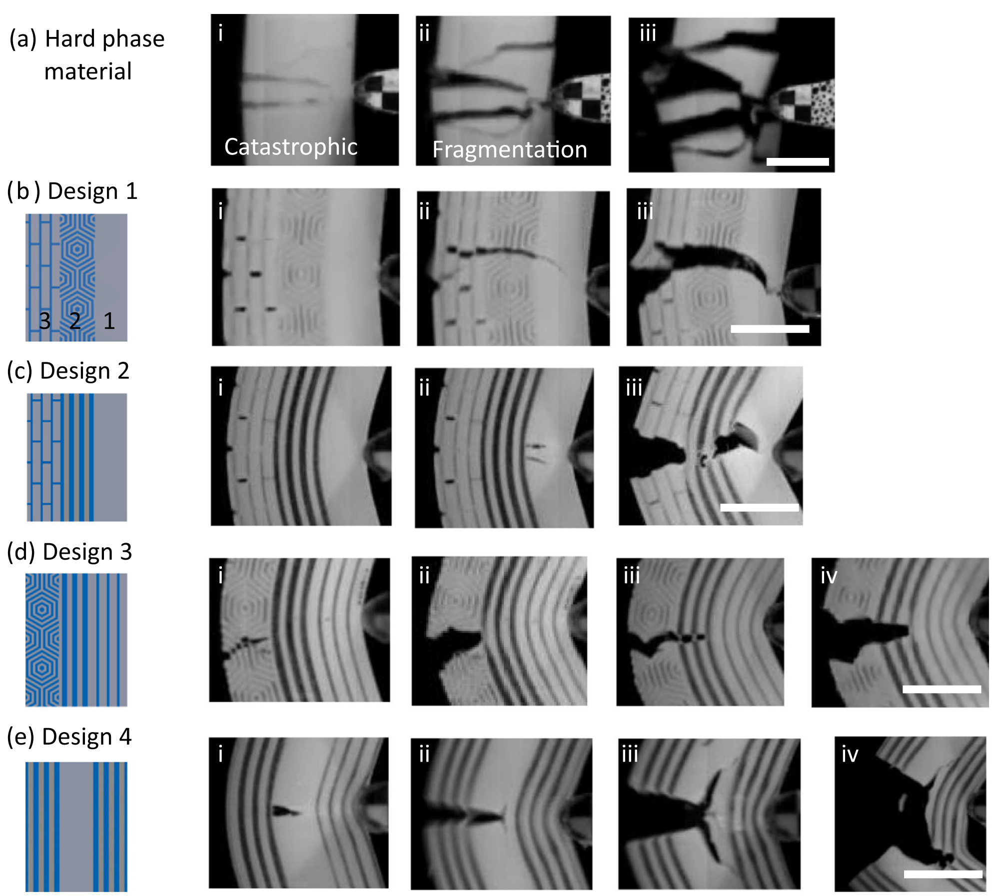

Fig. 8. Fracture pattern control enabled by the hybrid architectures. (a) A homogeneous beam composed by the hard phase exhibit catastrophic damage and fragmentation. (b) Crack initializes by microcracking in the third layer and propagates towards the first layer. (c) Crack initialize in layer 3, then initialize in layer 1, both subsequently propagates towards the center. (d) Crack propagates from layer 3 towards layer 1, with significant crack blunting bridging at layer 2. (e) Crack initialize in the center layer, which propagates towards layer 3, and then branches and propagates towards layer 1. Scale bars: 10 mm.

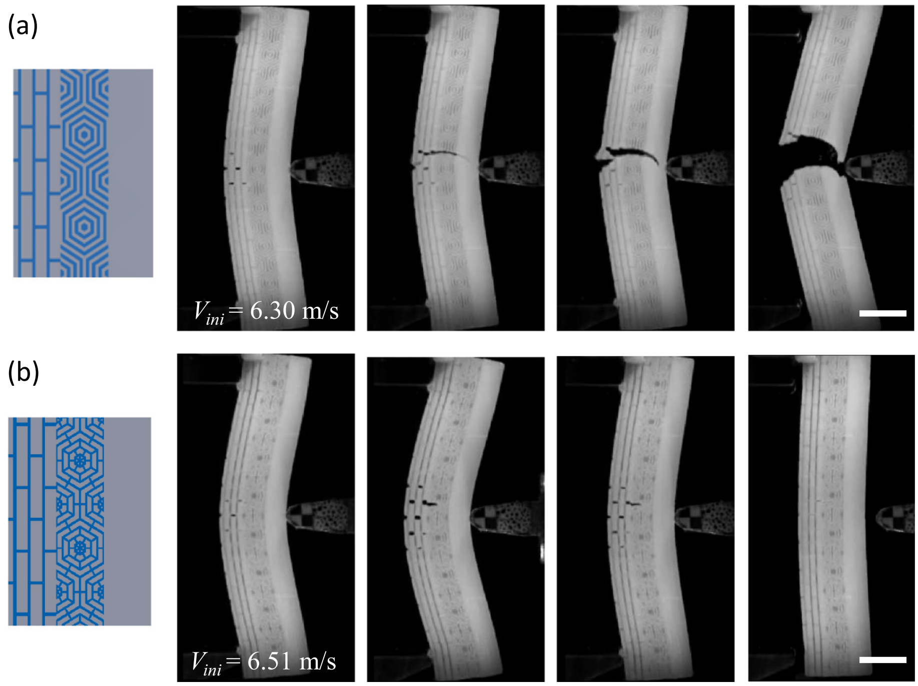

Fig. 9. Combining hierarchical design with hybrid design. (a) The crack penetrates the hybrid beam (with regular concentric hexagonal in the middle layer) at $V_{ini} = 6.3$ m/s. (b) Crack is captured by the same hybrid beam design (with a hierarchical concentric hexagonal counterpart in the middle layer) at $V_{ini} = 6.51$ m/s. Scale bars: 10 mm.

specimen's critical failure energy improves by more than 20% with only one unit cell thickness of the concentric hexagonal layer. This improvement arises from the enhanced failure force and fracture energy of the hierarchical structure as discussed in Section 3.3. These results suggest that combining hierarchical design with hybrid design offers one way of producing materials with better impact resistance.

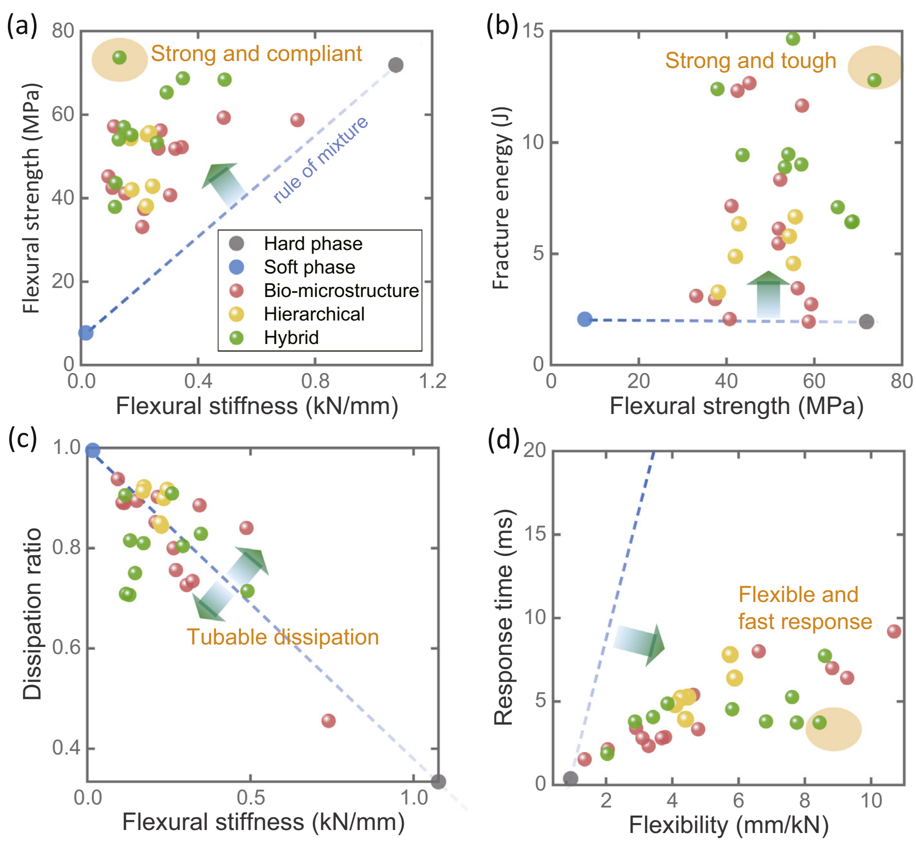

Fig. 10. Ashby plots demonstrating the capability of material architecture in expanding the material property space. Each point represents the performance of one architected material design obtained from at least 8 tests and is plotted using the average property value. The red, yellow, and green points represent the bioinspired microstructural elements, the hierarchical designs, and hybrid designs, respectively. The dashed lines represent the "rule of mixture" result. (For interpretation of the references to colour in this figure legend, the reader is referred to the web version of this article.)

3.6. Breaking the performance tradeoffs

To demonstrate the break of performance tradeoffs, the property space is visualized in Ashby plots in comparison with the rule of mixture results. Four conflicting requirements are considered here: 1) compliant and strong, 2) strong and tough, 3) stiff and dissipative, and 4) flexible and responsive. Fig. 10 shows that compared to the rule of mixture, proper architecture designs can improve the strength at a specific stiffness/compliance, improve the toughness at a specific strength, tune energy dissipation at a certain stiffness, and reduce the response time at certain flexibility. Thereby, the performance tradeoffs are surpassed, expanding the property space towards that beyond the constituents. More specifically, architected material that is as compliant as the soft phase but as strong as the hard phase is achieved (Fig. 10a). Architected materials that's 5% stronger and 7 times tougher than the hard phase is also obtained (Fig. 10b). Architected material that approach the high flexibility of the soft phase and high response rate of the hard phase is achieved (Fig. 10d). Note that the length scale of our specimens is in the μm to mm range. Aside from the nanoscale crack tolerance, the relationship between material structure and material property are largely scale free [56,70]. Thereby, studying the structure – property relationships at a length scale more operable would facilitate the understanding of material architecture at smaller length scales.

4. Conclusion

In summary, we have designed and fabricated specimens with microstructures mimicking nature's design motif and demonstrated that material architecture can be used to break the performance tradeoffs. The strength and toughness conflict has been largely tackled in previous studies, here, we further produce architected materials that break the performance tradeoffs between compliance and strength, stiffness and dissipation, and fast response and flexibility. Moreover, we show that ideal dynamic performance profiles with balanced stiffness/flexibility, strength, toughness, energy dissipation, and fast response are achievable by designing material microstructure. Combining the strain field visualization and theoretical analysis, we find the underlying mechanisms of balanced dynamic performance as follows.

(1) Flexibility and dissipation are promoted by large shear deformations in the soft phase.
(2) Strength and toughness arise from large local deformations (achieving a high stress level), cracks stopped at alternating soft and hard material, and enlarged fracture process zones (achieving large energy absorption).
(3) Fast response is facilitated by effective stress transfer between the soft and hard phase, together with a small to moderate energy dissipation ratio.

Moreover, material indices are proposed as quantitative parameters in the selection of material architecture. Overall performance parameters are proposed for structural components, as well as for applications like soft actuators and wearable electronics. Here, we focus on structures at the desktop scale with 3D printing, the proposed design strategies can be extended to different materials and length scales. Our study provides new opportunities to produce architected materials with ideal property combinations, which are of great interest for applications in armors, aerospace, wearable devices, and soft robotics.

CRediT authorship contribution statement

Zian Jia: Formal analysis, Data curation, Methodology, Investigation, Resources, Writing - original draft, Writing - review & editing, Visualization. **Yang Yu:** Data curation, Investigation, Resources, Writing - original draft, Visualization, Validation. **Lifeng Wang:** Conceptualization, Methodology, Investigation, Resources, Writing - original draft, Writing - review & editing, Validation, Supervision, Project administration, Funding acquisition.

Acknowledgements

The authors gratefully acknowledge the financial support from the National Science Foundation (CMMI-1462270). The authors thank Shaoyu Hou for assistance in the dynamic test. Zian Jia thanks A. Velasco-Hogan (University of California San Diego) for helpful discussions in preparing the manuscript. Yang Yu thanks the sponsorship from China Scholarship Council.

Appendix A. Supplementary data

Supplementary data to this article can be found online at https://doi.org/10.1016/j.matdes.2019.107650.

References

[1] M. Guvendiren, J. Molde, R.M. Soares, J. Kohn, Designing biomaterials for 3D printing, ACS Biomater Sci. Eng. 2 (10) (2016) 1679–1693.
[2] N.W. Bartlett, M.T. Tolley, J.T. Overvelde, J.C. Weaver, B. Mosadegh, K. Bertoldi, G.M. Whitesides, R.J. Wood, A 3D-printed, functionally graded soft robot powered by combustion, Science 349 (6244) (2015) 161–165.
[3] Y.L. Kong, I.A. Tamargo, H. Kim, B.N. Johnson, M.K. Gupta, T.-W. Koh, H.-A. Chin, D.A. Steingart, B.P. Rand, M.C. McAlpine, 3D printed quantum dot light-emitting diodes, Nano Lett. 14 (12) (2014) 7017–7023.
[4] S. Rudykh, C. Ortiz, M.C. Boyce, Flexibility and protection by design: imbricated hybrid microstructures of bio-inspired armor, Soft Matter 11 (13) (2015) 2547–2554.
[5] Z. Jia, T. Li, F.-p. Chiang, L. Wang, An experimental investigation of the temperature effect on the mechanics of carbon fiber reinforced polymer composites, Compos. Sci. Technol. 154 (2017) 53–63.
[6] M. Xia, J. Sanjayan, Method of formulating geopolymer for 3D printing for construction applications, Mater. Des. 110 (2016) 382–390.
[7] R.O. Ritchie, The conflicts between strength and toughness, Nat. Mater. 10 (11) (2011) 817.
[8] J.D. Currey, The design of mineralised hard tissues for their mechanical functions, J. Exp. Biol. 202 (23) (1999) 3285–3294.
[9] P. Zhang, M.A. Heyne, A.C. To, Biomimetic staggered composites with highly enhanced energy dissipation: modeling, 3D printing, and testing, J. Mech. Phys. Solids 83 (2015) 285–300.
[10] R. Lakes, High damping composite materials: effect of structural hierarchy, J. Compos. Mater. 36 (3) (2002) 287–297.
[11] J. Meaud, T. Sain, B. Yeom, S.J. Park, A.B. Shoultz, G. Hulbert, Z.-D. Ma, N.A. Kotov, A.J. Hart, E.M. Arruda, Simultaneously high stiffness and damping in nanoengineered microtruss composites, ACS Nano 8 (4) (2014) 3468–3475.
[12] A. Tonazzini, S. Mintchev, B. Schubert, B. Mazzolai, J. Shintake, D. Floreano, Variable stiffness fiber with self-healing capability, Adv. Mater. 28 (46) (2016) 10142–10148.
[13] M.F. Ashby*, Hybrids to fill holes in material property space, Philos. Mag. 85 (26–27) (2005) 3235–3257.
[14] M. Bechthold, J.C. Weaver, Materials science and architecture, Nat. Rev. Mater. 2 (12) (2017) 17082.
[15] T.-H. Huang, C.-S. Chen, S.-W. Chang, Microcrack patterns control the mechanical strength in the biocomposites, Mater. Des. 140 (2018) 505–515.
[16] H. Duan, Y. Han, W. Lu, L. Wang, J. Mao, D. Zhang, Configuration design and fabrication of laminated titanium matrix composites, Mater. Des. 99 (2016) 219–224.
[17] J.T. Overvelde, J.C. Weaver, C. Hoberman, K. Bertoldi, Rational design of reconfigurable prismatic architected materials, Nature 541 (7637) (2017) 347.
[18] E.L. Thomas, D.M. Anderson, C.S. Henkee, D. Hoffman, Periodic area-minimizing surfaces in block copolymers, Nature 334 (6183) (1988) 598–601.
[19] H.B. Yao, H.Y. Fang, Z.H. Tan, L.H. Wu, S.H. Yu, Biologically inspired, strong, transparent, and functional layered organic–inorganic hybrid films, Angew. Chem. Int. Ed. 49 (12) (2010) 2140–2145.
[20] G.M. Whitesides, B. Grzybowski, Self-assembly at all scales, Science 295 (5564) (2002) 2418–2421.
[21] C.N. Kaplan, W.L. Noorduin, L. Li, R. Sadza, L. Folkertsma, J. Aizenberg, L. Mahadevan, Controlled growth and form of precipitating microsculptures, Science 355 (6332) (2017) 1395–1399.
[22] J.R. Raney, B.G. Compton, J. Mueller, T.J. Ober, K. Shea, J.A. Lewis, Rotational 3D printing of damage-tolerant composites with programmable mechanics, Proc. Natl. Acad. Sci. 201715157 (2018).
[23] J.J. Martin, B.E. Fiore, R.M. Erb, Designing bioinspired composite reinforcement architectures via 3D magnetic printing, Nat. Commun. 6 (2015) 8641.
[24] J.A. Lewis, J.E. Smay, J. Stuecker, J. Cesarano, Direct ink writing of three-dimensional ceramic structures, J. Am. Ceram. Soc. 89 (12) (2006) 3599–3609.
[25] S. Bose, S. Vahabzadeh, A. Bandyopadhyay, Bone tissue engineering using 3D printing, Mater. Today 16 (12) (2013) 496–504.
[26] D.T. Pham, R.S. Gault, A comparison of rapid prototyping technologies, Int. J. Mach. Tools Manuf. 38 (10—11) (1998) 1257–1287.

[27] I. Stratasys, Fused deposition modelling for fast, safe plastic models, Twelfth Annual Conference on Computer Graphics, Chicago 1991, p. 326.
[28] M.R. Begley, N.R. Philips, B.G. Compton, D.V. Wilbrink, R.O. Ritchie, M. Utz, Micromechanical models to guide the development of synthetic 'brick and mortar' composites, J. Mech. Phys. Solids 60 (8) (2012) 1545–1560.
[29] X. Wu, M. Yang, F. Yuan, G. Wu, Y. Wei, X. Huang, Y. Zhu, Heterogeneous lamella structure unites ultrafine-grain strength with coarse-grain ductility, Proc. Natl. Acad. Sci. 112 (47) (2015) 14501–14505.
[30] J. Aizenberg, J.C. Weaver, M.S. Thanawala, V.C. Sundar, D.E. Morse, P. Fratzl, Skeleton of Euplectella sp.: structural hierarchy from the nanoscale to the macroscale, Science 309 (5732) (2005) 275–278.
[31] W. Clegg, K. Kendall, N.M. Alford, T. Button, J. Birchall, A simple way to make tough ceramics, Nature 347 (6292) (1990) 455–457.
[32] F. Bouville, E. Maire, S. Meille, B. Van de Moortèle, A.J. Stevenson, S. Deville, Strong, tough and stiff bioinspired ceramics from brittle constituents, Nat. Mater. 13 (5) (2014) 508–514.
[33] E. Munch, M.E. Launey, D.H. Alsem, E. Saiz, A.P. Tomsia, R.O. Ritchie, Tough, bio-inspired hybrid materials, Science 322 (5907) (2008) 1516–1520.
[34] F. Barthelat, H. Tang, P. Zavattieri, C.-M. Li, H. Espinosa, On the mechanics of mother-of-pearl: a key feature in the material hierarchical structure, J. Mech. Phys. Solids 55 (2) (2007) 306–337.
[35] A. Jackson, J. Vincent, R. Turner, The mechanical design of nacre, Proc. R. Soc. Lond. B Biol. Sci. 234 (1277) (1988) 415–440.
[36] Z. Jia, Y. Chen, H. Yang, L. Wang, Designing phononic crystals with wide and robust band gaps, Phys. Rev. Appl. 9 (4) (2018), 044021. .
[37] P. Liu, D. Zhu, Y. Yao, J. Wang, T.Q. Bui, Numerical simulation of ballistic impact behavior of bio-inspired scale-like protection system, Mater. Des. 99 (2016) 201–210.
[38] P. Fratzl, Biomimetic materials research: what can we really learn from nature's structural materials? J. R. Soc. Interface 4 (15) (2007) 637–642.
[39] R. Mirzaeifar, L.S. Dimas, Z. Qin, M.J. Buehler, Defect-tolerant bioinspired hierarchical composites: simulation and experiment, ACS Biomater Sci. Eng. 1 (5) (2015) 295–304.
[40] A. Velasco-Hogan, J. Xu, M.A. Meyers, Additive manufacturing as a method to design and optimize bioinspired structures, Adv. Mater. 1800940 (2018).
[41] M.A. Meyers, J. McKittrick, P.-Y. Chen, Structural biological materials: critical mechanics-materials connections, Science 339 (6121) (2013) 773–779.
[42] S.E. Naleway, M.M. Porter, J. McKittrick, M.A. Meyers, Structural design elements in biological materials: application to bioinspiration, Adv. Mater. 27 (37) (2015) 5455–5476.
[43] L.S. Dimas, M.J. Buehler, Modeling and additive manufacturing of bio-inspired composites with tunable fracture mechanical properties, Soft Matter 10 (25) (2014) 4436–4442.
[44] L.S. Dimas, G.H. Bratzel, I. Eylon, M.J. Buehler, Tough composites inspired by mineralized natural materials: computation, 3D printing, and testing, Adv. Funct. Mater. 23 (36) (2013) 4629–4638.
[45] G.X. Gu, F. Libonati, S.D. Wettermark, M.J. Buehler, Printing nature: unraveling the role of nacre's mineral bridges, J. Mech. Behav. Biomed. Mater. 76 (2017) 135–144.
[46] Y. Chen, L. Wang, Multiband wave filtering and wave guiding in bio-inspired hierarchical composites, Extreme Mech. Lett. 5 (2015) 18–24.
[47] G.X. Gu, M. Takaffoli, M.J. Buehler, Hierarchically enhanced impact resistance of bioinspired composites, Adv. Mater. 29 (28) (2017) 1700060.
[48] F. Libonati, G.X. Gu, Z. Qin, L. Vergani, M.J. Buehler, Bone-inspired materials by design: toughness amplification observed using 3D printing and testing, Adv. Eng. Mater. 18 (8) (2016) 1354–1363.
[49] F. Libonati, V. Cipriano, L. Vergani, M.J. Buehler, Computational framework to predict failure and performance of bone-inspired materials, ACS Biomater Sci. Eng. 3 (12) (2017) 3236–3243.
[50] D. Kokkinis, M. Schaffner, A.R. Studart, Multimaterial magnetically assisted 3D printing of composite materials, Nat. Commun. 6 (2015) 8643.
[51] A. Zaheri, J.S. Fenner, B.P. Russell, D. Restrepo, M. Daly, D. Wang, C. Hayashi, M.A. Meyers, P.D. Zavattieri, H.D. Espinosa, Revealing the mechanics of helicoidal composites through additive manufacturing and beetle developmental stage analysis, Adv. Funct. Mater. 1803073 (2018).
[52] Y. Chen, T. Li, Z. Jia, F. Scarpa, C.-W. Yao, L. Wang, 3D printed hierarchical honeycombs with shape integrity under large compressive deformations, Mater. Des. 137 (2018) 226–234.
[53] M.E. Launey, M.J. Buehler, R.O. Ritchie, On the mechanistic origins of toughness in bone, Annu. Rev. Mater. Res. 40 (2010) 25–53.
[54] J.-Y. Rho, L. Kuhn-Spearing, P. Zioupos, Mechanical properties and the hierarchical structure of bone, Med. Eng. Phys. 20 (2) (1998) 92–102.
[55] J. Buckwalter, M. Glimcher, R. Cooper, R. Recker, Bone biology. I: structure, blood supply, cells, matrix, and mineralization, Instr. Course Lect. 45 (1996) 371.
[56] H. Gao, Application of fracture mechanics concepts to hierarchical biomechanics of bone and bone-like materials, Int. J. Fract. 138 (1–4) (2006) 101.
[57] R. Lozano, L. Stevens, B.C. Thompson, K.J. Gilmore, R. Gorkin III, E.M. Stewart, M. in het Panhuis, M. Romero-Ortega, G.G. Wallace, 3D printing of layered brain-like structures using peptide modified gellan gum substrates, Biomaterials 67 (2015) 264–273.
[58] B.J. Bruet, J. Song, M.C. Boyce, C. Ortiz, Materials design principles of ancient fish armour, Nat. Mater. 7 (9) (2008) 748.
[59] J.C. Weaver, G.W. Milliron, A. Miserez, K. Evans-Lutterodt, S. Herrera, I. Gallana, W.J. Mershon, B. Swanson, P. Zavattieri, E. DiMasi, The stomatopod dactyl club: a formidable damage-tolerant biological hammer, Science 336 (6086) (2012) 1275–1280.
[60] A. Ajdari, B.H. Jahromi, J. Papadopoulos, H. Nayeb-Hashemi, A. Vaziri, Hierarchical honeycombs with tailorable properties, Int. J. Solids Struct. 49 (11—12) (2012) 1413–1419.
[61] L. Zhao, Q. Zheng, H. Fan, F. Jin, Hierarchical composite honeycombs, Mater. Des. 40 (2012) 124–129.
[62] C. Minas, D. Carnelli, E. Tervoort, A.R. Studart, 3D printing of emulsions and foams into hierarchical porous ceramics, Adv. Mater. 28 (45) (2016) 9993–9999.
[63] Y. Zhang, T. Liu, H. Ren, I. Maskery, I. Ashcroft, Dynamic compressive response of additively manufactured AlSi10Mg alloy hierarchical honeycomb structures, Compos. Struct. 195 (2018) 45–59.
[64] Q. Wu, A. Vaziri, M.E. Asl, R. Ghosh, Y. Gao, X. Wei, L. Ma, J. Xiong, L. Wu, Lattice materials with pyramidal hierarchy: systematic analysis and three dimensional failure mechanism maps, J. Mech. Phys. Solids 125 (2018) 112–144.
[65] L.R. Meza, A.J. Zelhofer, N. Clarke, A.J. Mateos, D.M. Kochmann, J.R. Greer, Resilient 3D hierarchical architected metamaterials, Proc. Natl. Acad. Sci. 112 (37) (2015) 11502–11507.
[66] J. Mueller, K. Shea, Stepwise graded struts for maximizing energy absorption in lattices, Extreme Mech. Lett. 25 (2018) 7–15.
[67] C. Schumacher, B. Bickel, J. Rys, S. Marschner, C. Daraio, M. Gross, Microstructures to control elasticity in 3D printing, ACM Trans. Graph. 34 (4) (2015) 136.
[68] A. Ion, J. Frohnhofen, L. Wall, R. Kovacs, M. Alistar, J. Lindsay, P. Lopes, H.-T. Chen, P. Baudisch, Metamaterial mechanisms, Proceedings of the 29th Annual Symposium on User Interface Software and Technology, ACM 2016, pp. 529–539.
[69] K. Lu, Stabilizing nanostructures in metals using grain and twin boundary architectures, Nat. Rev. Mater. 1 (5) (2016) 16019.
[70] Z. Zhang, Y.-W. Zhang, H. Gao, On optimal hierarchy of load-bearing biological materials, Proc. R. Soc. Lond. B Biol. Sci. 278 (1705) (2011) 519–525.
[71] J. Currey, Mechanical properties and adaptations of some less familiar bony tissues, J. Mech. Behav. Biomed. Mater. 3 (5) (2010) 357–372.
[72] Z. Jia, L. Wang, 3D Printing of Biomimetic Composites With Improved Fracture Toughness, (preprint) 2019https://doi.org/10.13140/RG.2.2.29406.48968.
[73] T. Yamamoto, T. Domon, S. Takahashi, N. Islam, R. Suzuki, Twisted plywood structure of an alternating lamellar pattern in cellular cementum of human teeth, Anat. Embryol. 202 (1) (2000) 25–30.
[74] A. Bigi, M. Burghammer, R. Falconi, M.H. Koch, S. Panzavolta, C. Riekel, Twisted plywood pattern of collagen fibrils in teleost scales: an X-ray diffraction investigation, J. Struct. Biol. 136 (2) (2001) 137–143.
[75] G. Agez, C. Bayon, M. Mitov, Multiwavelength micromirrors in the cuticle of scarab beetle Chrysina gloriosa, Acta Biomater. 48 (2017) 357–367.
[76] Z. Liu, D. Jiao, Z. Zhang, Remarkable shape memory effect of a natural biopolymer in aqueous environment, Biomaterials 65 (2015) 13–21.
[77] Z. Jia, Y. Yu, S. Hou, L. Wang, Biomimetic architected materials with improved dynamic performance, J. Mech. Phys. Solids 125 (2019) 178–197.
[78] X. Zeng, L. Ye, S. Yu, H. Li, R. Sun, J. Xu, C.-P. Wong, Artificial nacre-like papers based on noncovalent functionalized boron nitride nanosheets with excellent mechanical and thermally conductive properties, Nanoscale 7 (15) (2015) 6774–6781.
[79] J. Ryu, D. Hong, H.-W. Lee, S. Park, Practical considerations of Si-based anodes for lithium-ion battery applications, Nano Res. 10 (12) (2017) 3970–4002.
[80] M.F. Ashby, Materials Selection in Mechanical Design, Elsevier Science & Technology Books, 2016.
[81] R. Lakes, Materials with structural hierarchy, Nature 361 (6412) (1993) 511.